ChemComm

Cite this: *Chem. Commun.*, 2012, **48**, 3218–3220

www.rsc.org/chemcomm

COMMUNICATION

A DTTA-ligated uridine–quantum dot conjugate as a bimodal contrast agent for cellular imaging†

Junwon Park,‡[a] Sankarprasad Bhuniya,‡[a] Hyunseung Lee,[b] Young-Woock Noh,[c] Yong Taik Lim,[c] Jong Hwa Jung,[d] Kwan Soo Hong*[bc] and Jong Seung Kim*[a]

Received 3rd December 2011, Accepted 3rd February 2012
DOI: 10.1039/c2cc17555j

A uridine–quantum dot conjugate, a contrast agent for multimodal imaging, was synthesized. Its T_1 relaxivity was 655 and 571.2 mM^{-1} s^{-1} per particle at 36 °C in phosphate buffered saline at 60 and 200 MHz, respectively. *In vitro* multimodal images confirmed its uptake by RAW 264.7 cells.

Multifunctional nanoparticles engineered through nanoscale integration of multiple discrete components exhibit much more diverse and tunable optical, electronic, and magnetic properties than the corresponding bulk or single-component counterparts.[1] These superior properties are potentially useful in a variety of applications.[2] Recently, magnetofluorescent nanoparticles have attracted significant interest because of their great potential in diverse biomedical applications such as drug delivery, magnetic resonance (MR) and fluorescence (FR) imaging, and therapeutic systems.[3] Functionalized nanoparticles have become important for enhancing image contrast in medical diagnostics and are essential in molecular imaging.[4] Multimodal imaging agents have the potential to provide more than one signal from a biological sample, and thus, they enhance the visualization of biological processes. A number of multimodal probes with both paramagnetic and fluorescence signatures have been developed for cellular imaging and imaging in developmental biology, as MRI and optical techniques are excellent complementary imaging methods.[5–8] Previously we reported that DTTA-ligated uridine based amphiphilic MRI CAs are stable against biologically abundant Zn^{2+} and comparable with DTPA analogues Magnevist®/Omniscan®. This transmetallation stability also well reflected with the order of thermodynamic stability of the complexes.[9] Here, we report a new uridine-based bimodal contrast agent in conjunction with quantum dots (QDs) (Scheme 1). The QDs were employed as optical contrast agents because of their high brightness, long-term photo stability, and narrow, tunable emission spectrum.[10]

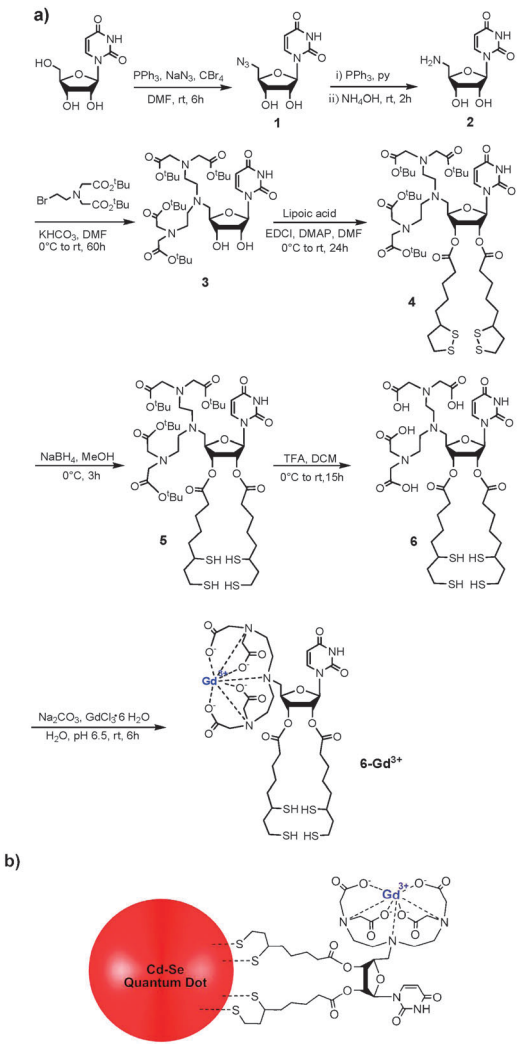

Scheme 1 Synthetic routes of (a) **6**-Gd^{3+} and (b) **6**-Gd^{3+}-QD.

The Gd^{3+} complex was synthesized as shown in Scheme 1. *N*-Alkylation of 5′-aminodeoxyuridine (**2**) with *N*,*N*-bis[(*tert*-butoxycarbonyl)methyl]-2-bromoethylamine in the presence of $KHCO_3$ at room temperature gave **3**. Further reaction of **3** with lipoic acid gave compound **4** in 45% yield. Subsequently,

[a] *Department of Chemistry, Korea University, Seoul 136-701, Korea. E-mail: jongskim@korea.ac.kr; Fax: +82-2-3290-3121*
[b] *Division of MR Research, Korea Basic Science Institute, Cheongwon 363-883, Korea*
[c] *Graduate School of Analytical Science and Technology, Chungnam National University, Daejeon 305-764, Korea*
[d] *Department of Chemistry and Research Institute of Natural Science, Gyeongsang National University, Jinju 660-701, Korea*
† Electronic supplementary information (ESI) available: Experimental details, synthesis, spectroscopic data, and NMR data. See DOI: 10.1039/c2cc17555j
‡ These authors contributed equally to this work.

S–S bond reduction of **4** by $NaBH_4$ followed by BOC deprotection afforded **6** where a diethylene-triaminotetraacetic acid (DTTA) group acted as the binding site for Gd^{3+}. The ligand **6** was complexed with $GdCl_3$ in ultrapure water with a pH of 6.5 to yield an anionic complex (**6**-Gd^{3+}) (Scheme 1(a)). Next, the **6**-Gd^{3+} was attached to CdSe/ZnS QDs (λ_{max}: 655 nm) by a ligand exchange protocol reported previously.[11]

QDs (1.0 mL, 1.0 μM, Invetrogen) in decane were added to an aqueous ethanol solution of **6**-Gd^{3+} (100 mg, 90 μmol) and stirred for 10 h at 80 °C. After cooling the reaction mixture to room temperature, filtering the precipitates from the solution, and washing with cold ethanol, **6**-Gd^{3+}-QDs were obtained as pale yellow solids. This new multimodal contrast agent has core Cd–Se QDs incorporated in the centre with the paramagnetic uridine-based Gd^{3+} complex (**6**-Gd^{3+}) coated on the surface to create the potential for bimodal MRI and fluorescence imaging in biological systems.

To confirm the binding of **6**-Gd^{3+} on QD surface, the UV-Vis absorption spectra of **6**-Gd^{3+} were measured before and after QD attachment (Fig. S8, ESI†).[12] Based on the UV-Vis absorption spectroscopy results, the number of **6**-Gd^{3+} moieties per QD particle was estimated to be approximately 56 ± 6. The fluorescent property of QD remains unaltered even in conjunction with **6**-Gd^{3+} (Fig. S9–S11, ESI†). In addition, we obtained TEM images of **6**-Gd^{3+}-QD, which also verified that **6**-Gd^{3+}s are attached to the QD surface as shown in Fig. 1. Furthermore, electron energy loss spectroscopy (EELS),[13] which can provide elemental and chemical information with high spatial resolution, was utilized to characterize **6**-Gd^{3+}-QD and the results are shown in Fig. 1(B) and Fig. S12 (ESI†). The **6**-Gd^{3+}-QD contains the elements C, O, Cd, and Gd. This proves that **6**-Gd^{3+} is homogenously attached to the external surface of the QD. By the dynamic light scattering (DLS) method (Fig. 1(A)), the average diameter of the **6**-Gd^{3+}-QD was found to be *ca.* 160 nm, which is in good agreement with the TEM results.

To verify the ability of the **6**-Gd^{3+}-QD to act as an MRI contrast agent, we measured the T_1 relaxivity (r_1) of **6**-Gd^{3+}-QD in phosphate buffered saline. The T_1 relaxivity (r_1) is calculated from the linear fitting of the measured R_1 ($=1/T_1$) data *vs.* Gd

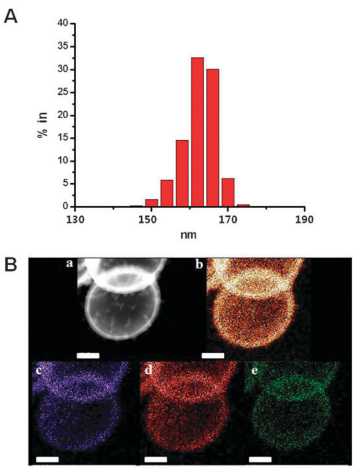

Fig. 1 DLS and TEM characterization of **6**-Gd^{3+}-QD. (A) DLS of **6**-Gd^{3+}-QD, (B) TEM images of **6**-Gd^{3+}-QD: (a) TEM image of **6**-Gd^{3+}-QD, (b) C component, (c) O component, (d) Cd component, and (e) Gd component. Scale bars: 50 nm.

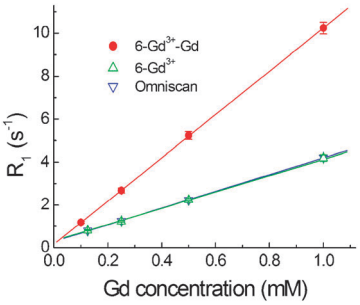

Fig. 2 T_1 relaxivity measurement of the **6**-Gd^{3+}-QD. Gd-concentration dependence of the measured relaxation rates (R_1) of the **6**-Gd^{3+}-QD are shown and are compared with those of clinically available T_1 contrast agent, Omniscan®, and **6**-Gd^{3+} at 200 MHz and 36 °C.

concentration (Fig. 2). The measured r_1 value of **6**-Gd^{3+}-QD at 200 MHz was 10.2 ± 0.1 mM^{-1} s^{-1} per Gd^{3+} ion (11.7 ± 0.1 mM^{-1} s^{-1} at 60 MHz, data not shown), which is 2.5-fold higher than the r_1 values of clinically used T_1 CA Omniscan® (Gd-DTPA-BMA; Amersham, USA) and the free ligand **6**-Gd^{3+} (r_1 values of Omniscan® and **6**-Gd^{3+} are ~4.2 mM^{-1} s^{-1}). The relaxivity of **6**-Gd^{3+}-QD per QD particle was 571.2 mM^{-1} s^{-1} at 200 MHz, which was significantly higher than those reported in the case of QD-Gd^{3+} nano-particles.[14] It is assumed that this significantly higher r_1 value of **6**-Gd^{3+}-QD is because of restricted molecular tumbling and reduced global rotational motion due to the conjugation of the complex on the QD surface, which enhances the r_1 of each complex.[15] These results indicate that the high T_1 relaxivity per particle in cellular imaging application after *in vivo* or *in vitro* labeling of specific cells with **6**-Gd^{3+}-QD could facilitate highly sensitive MRI cell tracking with minimal cell labeling.

To demonstrate the application of the **6**-Gd^{3+}-QD as a sensitive MR/FR cellular imaging probe, we first investigated cell biocompatibility of the nano-constructed **6**-Gd^{3+}-QD using a murine macrophage cell line (RAW 264.7). As shown in Fig. 3, we observed by comparing with the control that labeling of RAW 264.7 cells with **6**-Gd^{3+}-QD and incubation for 24 h does not significantly influence the cell viability at Gd^{3+} concentrations lower than 11.2 μM. No significant **6**-Gd^{3+}-QD cytotoxicity was observed in RAW 264.7 cells at Gd^{3+} concentrations lower than 11.2 μM after labeling in culture media for 24 h.

Intracellular delivery of **6**-Gd^{3+}-QD to RAW 264.7 cells was easily investigated by fluorescence microscopy (Fig. 4) and flow cytometry (Fig. S13, ESI†), and the extent of labeled **6**-Gd^{3+}-QD could be measured on the basis of the fluorescence intensity from QDs.

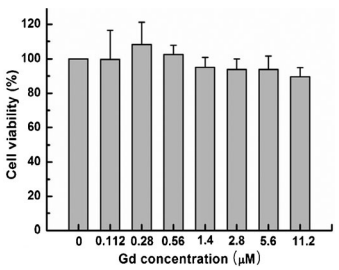

Fig. 3 Measurement of cytotoxicity of **6**-Gd^{3+}-QD in RAW 264.7 cells.

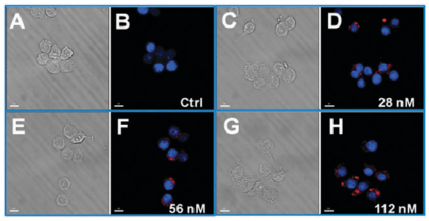

Fig. 4 Fluorescence microscopic images of RAW 264.7 cells labeled with **6**-Gd^{3+}-QD. Bright-field microscopy images (A, C, E, G) and fluorescence microscopic images (B, D, F, H) with blue (DAPI for nucleus) and red (for **6**-Gd^{3+}-QD) are shown to be dependent on QD concentration in cell culture media. Images were acquired using 490/20 nm excitation and fluorescent emission windows of 617/73 nm (red). Scale bar: 10 μm.

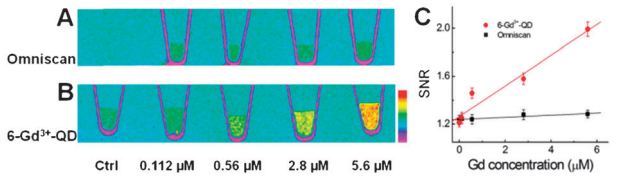

Fig. 5 High-performance MR/FR dual imaging properties of **6**-Gd^{3+}-QD. T_1-weighted MR images, at 4.7 T and 36 °C, of RAW 264.7 cells (10^7 cells each) labeled with Omniscan® (A) and **6**-Gd^{3+}-QD in pseudo color (B) in function of Gd^{3+} concentration, and signal-to-noise ratios (SNRs) are compared to (C).

Efficiency of RAW MRI T_1 complexes such as Omniscan® and Magnevist® for nonspecific *in vitro* cell labeling is rather low for MRI. The cell-labeling efficiency of **6**-Gd^{3+}-QD was compared with that of the commercial MR contrast agent, Omniscan®. As shown in Fig. 5, the T_1 shortening effect in **6**-Gd^{3+}-QD-labeled cells (Fig. 5(B)) is more dominant than that in Omniscan®-labeled cells (Fig. 5(A)). A notable fact is that the positive contrast enhancement by using **6**-Gd^{3+}-QD at 0.112 μM of Gd^{3+} was similar to that achieved by using Omniscan® at 5.6 μM. This implies that the labeling efficiency of **6**-Gd^{3+}-QD was about 20-times higher than that of commercial T_1 CA of Omniscan®, after taking into account the 2.4-fold higher T_1 relaxivity of **6**-Gd^{3+}-QD. The SNR value measured as a T_1 positive contrast effect from MR images with **6**-Gd^{3+}-QD-labeled macrophages (10^7 cells) markedly increased with Gd^{3+} (or QD) concentrations lower than 5.6 μM Gd^{3+} (= 100 nM QD) in the cell culture media, while there was little change with Omniscan® (Fig. 5(C)). By the conjugation of Gd^{3+} complex with QD nanoparticles, the labeling efficiency in macrophages dramatically increased, resulting in a positive contrast of *in vitro*/*in vivo* MR images due to accumulated cellular labeling of the bimodal MR/FR imaging probe.

Although we assumed that the considerable increase in the efficiency of intracellular delivery of **6**-Gd^{3+}-QD in macrophages may result from the phagocytosis of **6**-Gd^{3+}-QD, the actual mechanism of interaction of the QD complexes with the cell membrane and their entry into the cells is a complex process that includes nonreceptor-mediated endocytosis.[16] This mechanism will be investigated in the future.

In summary, a bimodal fluorescent MR contrast agent, **6**-Gd^{3+}-QD, has been developed by conjugation of CdSe/ZnS QDs with a uridine-based paramagnetic complex (**6**-Gd^{3+}). The relaxivities of **6**-Gd^{3+}-QD are 655 and 572 mM^{-1} s^{-1} per particle at 60 and 200 MHz, respectively. **6**-Gd^{3+}-QD can smoothly penetrate the cell surface and can be delivered into the intracellular regions of RAW 264.7 cells. Further, **6**-Gd^{3+}-QD facilitates high-performance MR and fluorescence imaging. Since this QD-conjugated T_1 contrast agent easily labeled macrophages, which are phagocytic cells and since it had low cytotoxicity, **6**-Gd^{3+}-QD as a bimodal MR/FR cellular imaging nanoprobe can be used to probe similar phagocyte cells such as T cells, B cells, neutrophils, granulocytes, and dendritic cells.

This work was supported by a grant from the CRI project (No. 2011-0000420) (JSK), (2011-0029263) (KSH), Korea Basic Science Institute (T31403) (KSH) and WCU project (R32-2008-000-20003-0) (JHJ) of Korea.

Notes and references

1 Y. D. Jin and X. H. Gao, *Nat. Nanotechnol.*, 2009, **4**, 571.
2 (*a*) X. H. Gao, Y. Y. Cui, R. M. Levenson, L. W. K. Chung and S. M. Nie, *Nat. Biotechnol.*, 2004, **22**, 969; (*b*) V. Bagalkot, L. Zhang, E. Levy-Nissenbaum, S. Jon, P. W. Kantoff, R. Langer and O. C. Farokhzad, *Nano Lett.*, 2007, **7**, 3065.
3 (*a*) J. H. Gao, H. W. Gu and B. Xu, *Acc. Chem. Res.*, 2009, **42**, 1097; (*b*) E. H. Moriyama, G. Zhang and B. C. Wilson, *Clin. Pharmacol. Ther.*, 2008, **84**, 267; (*c*) C. Xu, J. Xie, D. Ho, C. Wang, N. Kohler, E. G. Walsh, J. R. Morgan, Y. E. Chin and S. Sun, *Angew. Chem., Int. Ed.*, 2007, **46**, 173; (*d*) J. H. Choi, F. T. Nguyen, P. W. Barone, D. A. Heller, A. E. Moll, D. Patel, S. A. Boppart and M. S. Strano, *Nano Lett.*, 2007, **7**, 861.
4 (*a*) N. L. Rosi and C. A. Mirkin, *Chem. Rev.*, 2005, **105**, 1547; (*b*) Y. Song, X. Xu, K. Macrenaris, X.-Q. Zhang, C. Markin and T. J. Meade, *Angew. Chem., Int. Ed.*, 2009, **48**, 9143.
5 M. M. Hüber, A. B. Staubli, K. Kustedjo, M. H. B. Gray, J. Shih, S. E. Fraser, R. E. Jacobs and T. J. Meade, *Bioconjugate Chem.*, 1998, **9**, 242.
6 C. Brekke, S. C. Morgan, A. S. Lowe, T. J. Meade, J. Price, S. C. Williams and M. Modo, *NMR Biomed.*, 2007, **20**, 77.
7 M. Modo, K. Mellodew, D. Cash, S. E. Fraser, T. J. Meade, J. Price and S. C. Williams, *NeuroImage*, 2004, **21**, 311.
8 A. Dirksen, S. Langereis, B. F. M. de Waal, M. H. P. van Genderen, E. W. Meijer, Q. G. de Lussanet and T. M. Hackeng, *Org. Lett.*, 2004, **6**, 4857.
9 (*a*) S. Bhuniya, H. Moon, H. Lee, K. S. Hong, S. Lee, D.-Y. Yu and J. S. Kim, *Biomaterials*, 2011, **32**, 6533; (*b*) R. N. Muller, B. Radüchel, S. Laurent, J. Platzek, C. Piérart, P. Mareski and L. V. Elst, *Eur. J. Inorg. Chem.*, 1999, 1949.
10 (*a*) W. C. W. Chan and S. Nie, *Science*, 1998, **281**, 2016; (*b*) M. Dahan, S. Levi, C. Luccardini, P. Rostaing, B. Riveau and A. Triller, *Science*, 2003, **302**, 442.
11 W. Liu, M. Howarth, A. B. Greytak, Y. Zheng, D. G. Nocera, A. Y. Ting and M. G. Bawendi, *J. Am. Chem. Soc.*, 2008, **130**, 1274.
12 J. Takashi, Y. Yoshichika, F. Fuji, Y. Komai, J. Seki and A. Seiyama, *Chem. Commun.*, 2008, 5764.
13 J. H. Jung, K. Yoshida and T. Shimizu, *Langmuir*, 2002, **18**, 8724.
14 (*a*) H. Yang, S. Santra, G. A. Walter and P. H. Holloway, *Adv. Mater.*, 2006, **18**, 2890; (*b*) G. A. F. van Tilborg, W. J. M. Mulder, P. T. K. Chin, G. Storm, C. P. Reutelingsperger, K. Nicolay and G. J. Strijkers, *Bioconjugate Chem.*, 2006, **17**, 865; (*c*) G. J. Stasiuk, S. Tamang, D. Imbert, C. Poillot, M. Giardiello, C. Tisseyre, E. L. Barbier, P. H. Fries, M. de Waard, P. Reiss and M. Mazzanti, *ACS Nano*, 2011, **5**, 8193.
15 P. Caravan, J. J. Ellison, T. J. McMurry and R. B. Lauffer, *Chem. Rev.*, 1999, **99**, 2293.
16 H. Huang, E. Pierstorff, E. Osawa and D. Ho, *Nano Lett.*, 2007, **7**, 3305.

